



This is the peer reviewed version of the following article:

Gao, N., Geyer, F., Pilat, D. W., Wooh, S., Vollmer, D., Butt, H.-J., et al. (2018). How drops start sliding over solid surfaces. *Nature Physics*, 14(2), 191-196. doi:10.1038/NPHYS4305.

, which has been published in final form at: [10.1038/NPHYS4305](https://doi.org/10.1038/NPHYS4305)

Supplementary Material

How drops start sliding over solid surfaces

Nan Gao, Florian Geyer, Dominik W. Pilat, Sanghyuk Wooh, Doris Vollmer, Hans-Jürgen Butt & Rüdiger Berger

How drops start sliding over solid surfaces

Nan Gao^{1,2}, Florian Geyer¹, Dominik Pilat¹, Sanghyuk Wooh¹, Doris Vollmer¹, Hans-Jürgen Butt¹,
Rüdiger Berger¹

1 Max Planck Institute for Polymer Research, Ackermannweg 10, 55128 Mainz, Germany

2 Fudan University, 220 Handan Road, Shanghai 200433, People’s Republic of China

General: We used the word “sliding” in our manuscript according to the Merriam-Webster dictionary: to “move smoothly along a surface”. The latter includes also partial rolling.

Preparation of solid surfaces and liquid drops

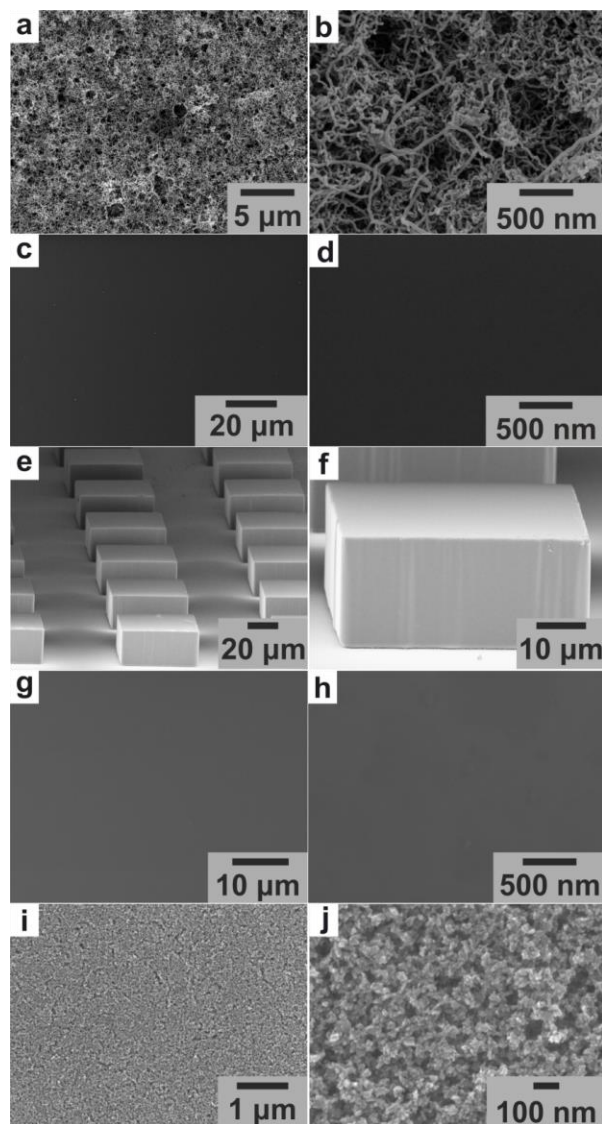


Figure S1. Scanning Electron Microscopic Images of the Solid Substrates. **a-b**, Fluorinated silicon nanofilaments coated on a glass slide. **c-d**, Fluorinated Si wafer. **e-f**, Fluorinated SU-8 pillars fabricated on a glass slide. (**g & h**): PDMS coated on a glass slide. **i-j**, Fluorinated TiO₂ nanoparticles coated on a silicon wafer. The images on the right are magnified versions of the images on the left. The brightness of the images was adjusted for observation. Images were taken with a Zeiss LEO 1530 GEMINI SEM. All samples except the fluorinated silicon wafer and TiO₂ surfaces were sputtered with Pt using BalTec MED 020 modular high vacuum coating system (argon at 2×10^{-5} bar, 60 mA) to avoid charging of the samples during Scanning Electron Microscopy imaging.

Force Measurement

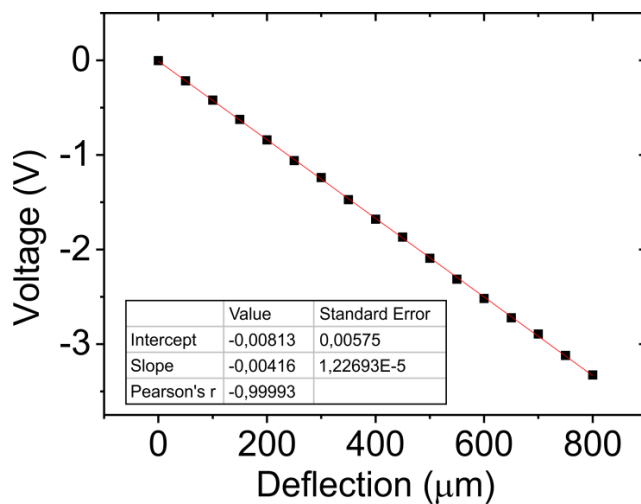


Figure S2. Plot of the sensitivity of the laser deflection system. The deflection of the capillary, D , was changed in steps of $50 \mu\text{m}$ using a micromanipulator. For this calibration we calculated $S = U / D = -4.16 \times 10^{-3} \pm 0.01 \times 10^{-3} \text{ V}/\mu\text{m}$.

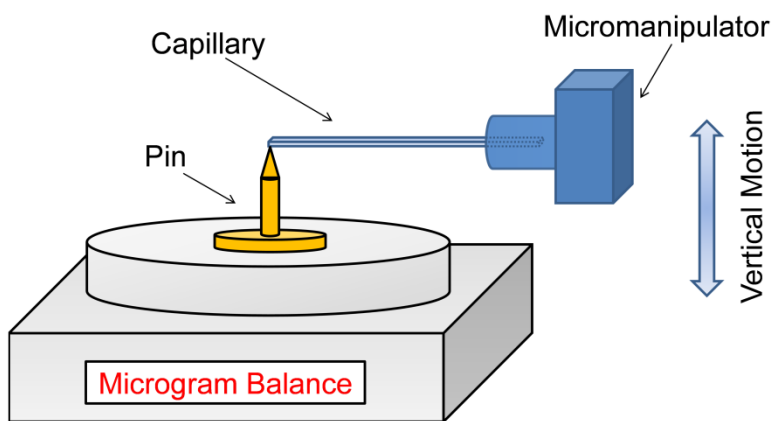


Figure S3. Schematic of spring constant calibration of a capillary. The micromanipulator was moved vertically, in steps of $50 \mu\text{m}$ resulting in a deflection of the capillary in opposite direction.

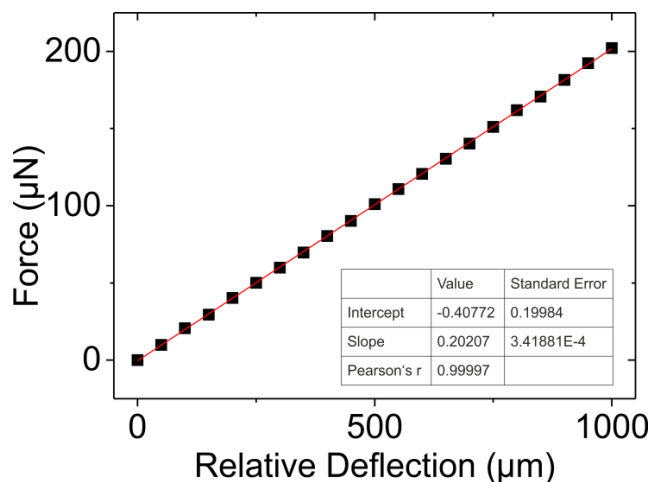


Figure S4. A representative plot of the spring constant of the glass capillary. The deflection, D , of the capillary was changed in steps of $50 \mu\text{m}$ using the micromanipulator. For this calibration we calculated $\kappa = F / D = 0.202 \text{ N/m}$ with a Pearson $r = 0.9999$.

Development of the lateral adhesion force, contact width and length, contact angles and the k factor

k factor

The lateral adhesion forces measured by means of the laser deflection system have been compared with the values calculated using:

$$F_{LA} = k \cdot L \cdot \gamma \cdot (\cos \theta_{Rear} - \cos \theta_{Front}) \quad \text{Eq. 9}$$

This equation is derived for sessile liquid drops overcoming retentive forces on solid surfaces⁹⁻¹⁴. The dimensionless k factor accounts for the precise shape of the drop. The values of k were adopted to be 1 in our calculations. Dividing the measured forces F_{LA} by $L \cdot \gamma \cdot (\cos \theta_{Rear} - \cos \theta_{Front})$ the k factor can be calculated. Here, the measured values for L , θ_{Rear} and θ_{Front} are used. Fig. S5d shows an example of the k factor development over an entire experiment. In the static and transition regimes, the k factor changes non-monotonously, varying between 0.9 and 1.6. In the kinetic regime, the k value stays between 1.4 and 1.5. Practically, the k factor is sensitive to any change in contact angles and contact widths caused by surface inhomogeneities

on the (sub-) micrometer length scale that can cause pinning and depinning, of the contact line. Yet setting $k = 1$ leads to a parameter-free approximation of the lateral adhesion force for general understanding.

In addition, we calculated the average k factor in the kinetic regime by dividing the measured and calculated adhesion forces within the last 3 - 5 seconds of the measurement. Table S1 gives the averaged k factors in the kinetic regime, showing that the k factors vary from sample to sample. However, values within the range of 1.0 - 1.5 are typically obtained.

Table S1. k factor averaged of the last 3 - 5 seconds in the kinetic regime, $v = 0.2$ mm/s.

	k factor
Water fluorinated TiO ₂ nanostructures	1.48 ± 0.06
Water on fluorinated SU-8 Pillars	1.23 ± 0.06
Water on fluorinated Si	1.45 ± 0.01
Water on PDMS	1.09 ± 0.02
Water on fluorinated silicone nanofilaments	1.43 ± 0.23
Ionic Liquid on fluorinated Si	1.21 ± 0.03
Hexadecane on fluorinated Si	1.46 ± 0.03

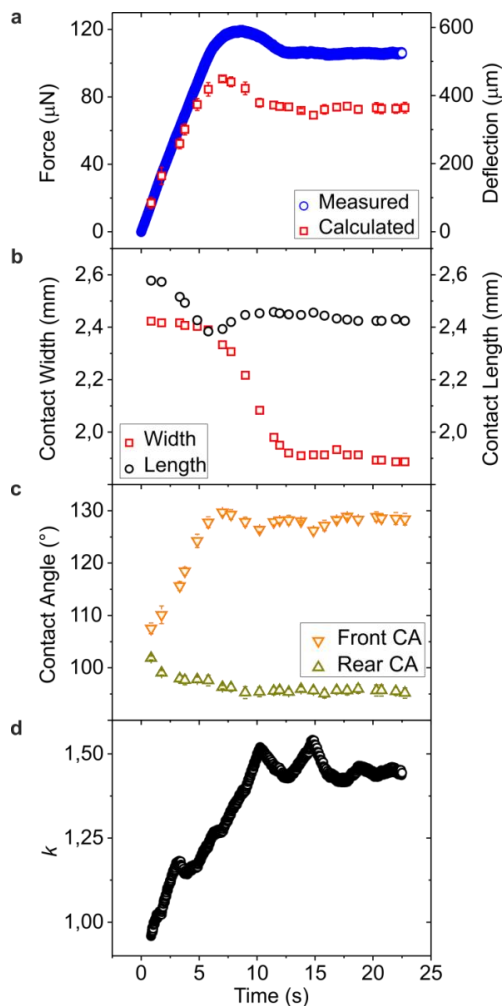


Figure S5. a, Lateral adhesion forces between a water drop ($\approx 7.5 \mu\text{L}$) and a fluorinated silicon wafer. The measurement was performed while the linear stage moved at a constant velocity of $202 \mu\text{m/s}$. The surface tension of water for the calculation of the lateral adhesion forces was 73.5 mN/m . **b**, Evolution of the contact widths and lengths of the drop during the force measurement. The contact length decreases before F_{THRD} is reached. Likely, this is a result of the detaching (depinning) of the receding side of the drop that takes place before the advancing side starts moving. See the movie clips (water on Si at $t = -11792 \text{ ms}$: Supplementary Video/ Movie - Water on Si). **c**, Evolution of the front and rear contact angles during the force measurement. **d**, k factors obtained by dividing the measured forces by the calculated forces from **a**. The result is a 1000-point interpolation to guide the eye.

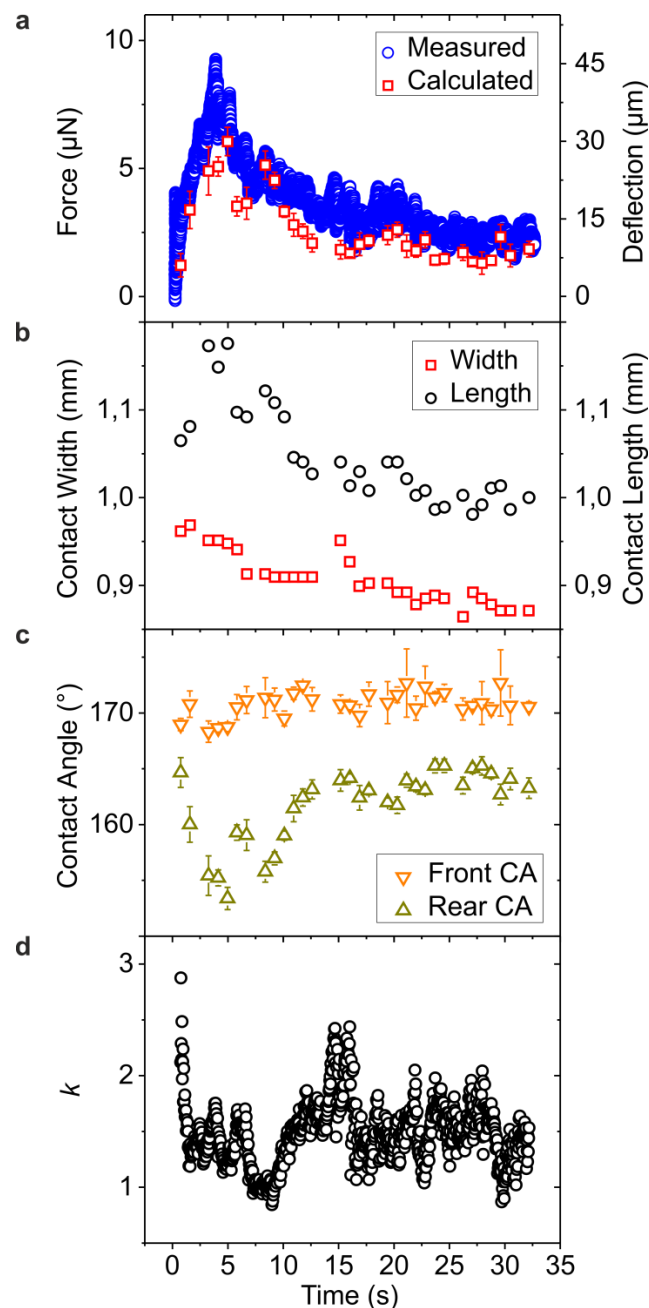


Figure S6. *a*, Lateral adhesion forces between a water drop ($\approx 7.5 \mu\text{L}$) and a fluorinated silicone nanofilament substrate. The measurement was performed while the linear stage moved at a constant velocity of $202 \mu\text{m/s}$. The surface tension of water for the calculation of the lateral adhesion forces was 73.5 mN/m . *b*, Evolution of the contact widths and lengths of the drop during the force measurement. *c*, Evolution of the front and rear contact angles during the force measurement. *d*, *k* factors obtained by dividing the measured forces by the calculated forces from *a*. The result is a 1000-point interpolation to guide the eye.

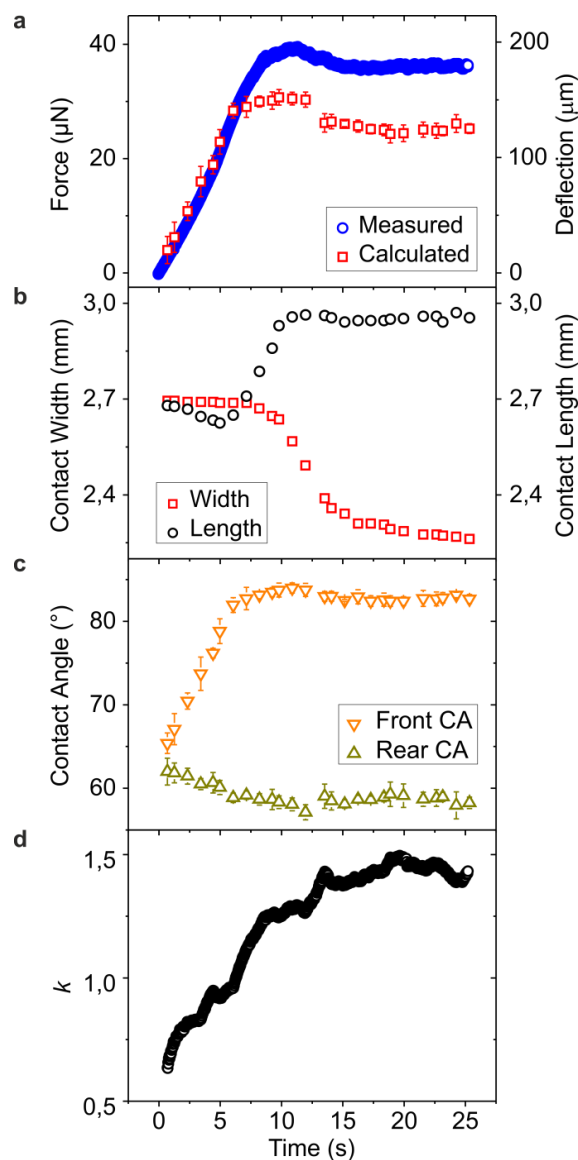


Figure S7. a, Lateral adhesion forces between a hexadecane drop ($\approx 3 \mu\text{L}$) and a fluorinated Si wafer. The measurement was performed while the linear stage moved at a constant velocity of $202 \mu\text{m/s}$. The surface tension of hexadecane for the calculation of the lateral adhesion forces was 27.5 mN/m . **b**, Evolution of the contact widths and lengths of the drop during the force measurement. The contact length decreases before F_{THRD} is reached. Likely, this is a result of the detaching (depinning) of the receding side of the drop that takes place before the advancing side starts moving. See the movie clips (hexadecane on Si at $t = -7996 \pm 100 \text{ ms}$: Supplementary Video/ Movie - Hexadecane on Si). **c**, Evolution of the front and rear contact angles during the force measurement. **d**, k factors obtained by dividing the measured forces by the calculated forces from **a**. The result is a 1000-point interpolation to guide the eye.

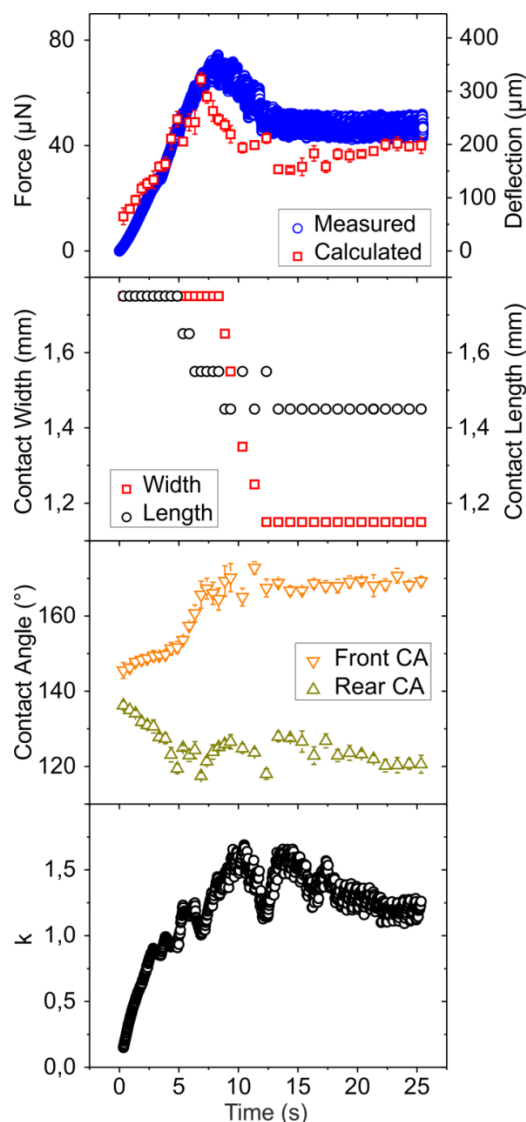


Figure S8. a, Lateral adhesion forces between a water drop ($\approx 7.5 \mu\text{L}$) and a fluorinated array of SU-8 pillars. The measurement was performed while the linear stage moved at a constant velocity of $202 \mu\text{m/s}$. The surface tension of water for the calculation of the lateral adhesion forces was 73.5 mN/m . **b**, Evolution of the contact widths and lengths of the drop during the force measurement. The contact length decreases before F_{THRD} is reached. Likely, this is a result of the detaching (depinning) of the receding side of the drop that takes place before the advancing side starts moving. Note that water droplets are in the Cassie-state for such circumstances. See the movie clips (water on Si at $t = -72 \text{ ms}$ to $t = +48 \text{ ms}$: Supplementary Video/ Movie - Water on SU-8). **c**, Evolution of the front and rear contact angles during the force measurement. **d**, k factors obtained by dividing the measured forces by the calculated forces from **a**. The result is a 1000-point interpolation to guide the eye.

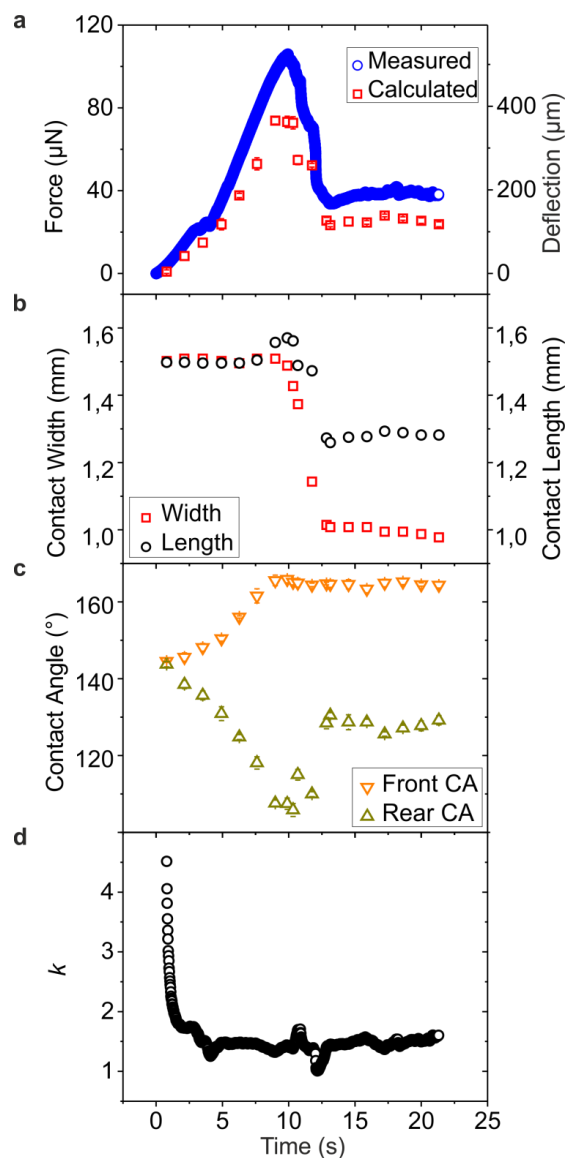


Figure S9. *a*, Lateral adhesion forces between a water drop ($\approx 7.5 \mu\text{L}$) and fluorinated TiO_2 nanoparticles on a Si wafer. The measurement was performed while the linear stage moved at a constant velocity of $202 \mu\text{m/s}$. The surface tension of water for the calculation of the lateral adhesion forces was 73.5 mN/m . *b*, Evolution of the contact widths and lengths of the drop during the force measurement. *c*, Evolution of the front and rear contact angles during the force measurement. *d*, *k* factors obtained by dividing the measured forces by the calculated forces from *a*. The result is a 1000-point interpolation to guide the eye.

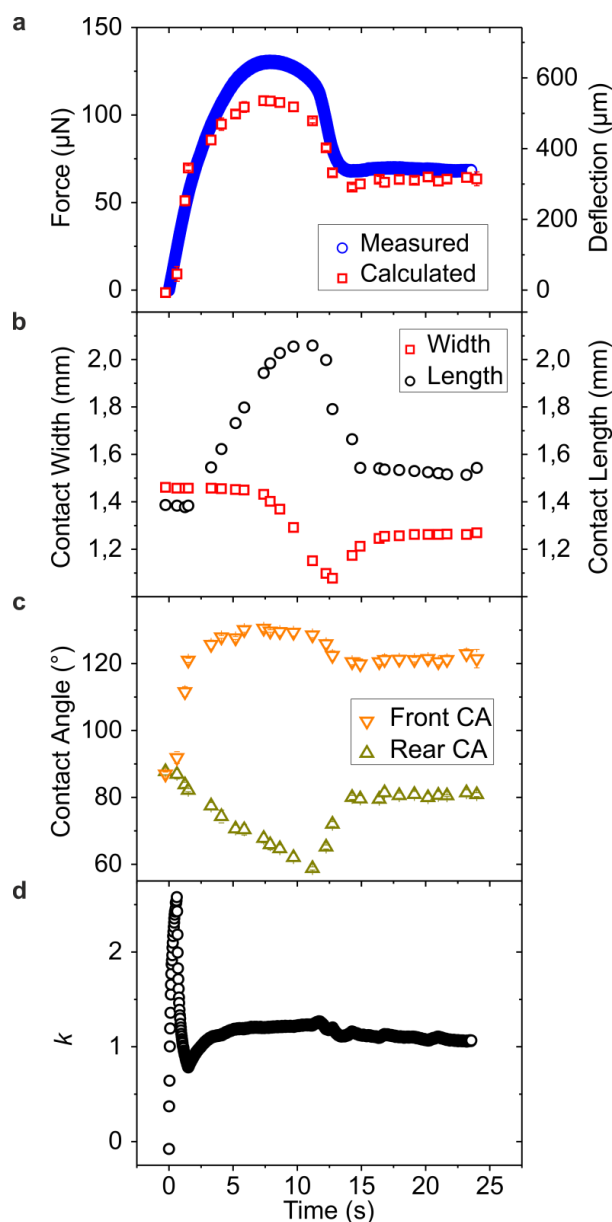


Figure S10. *a*, Lateral adhesion forces between a water drop ($\approx 1.5 \mu\text{L}$) and PDMS on a glass slide. The measurement was performed while the linear stage moved at a constant velocity of $202 \mu\text{m/s}$. The surface tension of water for the calculation of the lateral adhesion forces was 73.5 mN/m . *b*, Evolution of the contact widths and lengths of the drop during the force measurement. *c*, Evolution of the front and rear contact angles during the force measurement. *d*, *k* factors obtained by dividing the measured forces by the calculated forces from *a*. The result is a 1000-point interpolation to guide the eye.

Comparison of lateral adhesion forces for conventionally crosslinked PDMS and liquid-like PDMS surfaces

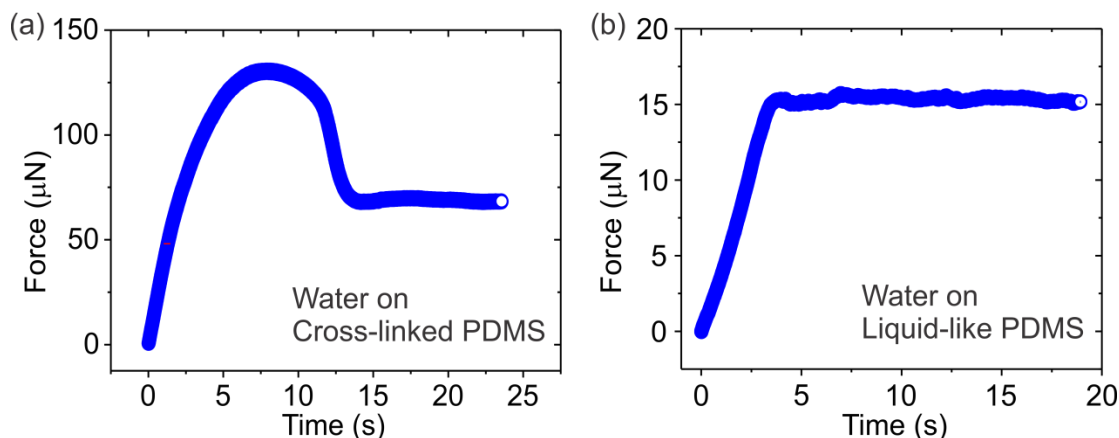


Figure S11. Comparison of the lateral adhesion forces between a water drop and a glass slide coated with (a) cross-linked PDMS and (b) liquid-like PDMS. The flexibility of the O-Si-O bonds confers high mobility to PDMS chains. As only one end of silicone oil is covalently grafted on the substrate, the remaining part of the silicone oil keeps its high mobility with rotational and/or bending motion. These grafted layers are rotationally dynamic and behave “liquid-like”. Water drops slide off these “liquid-like” surfaces when tilting the surfaces by a few degrees. **a**, The measurement was performed at a constant velocity of $202 \mu\text{m/s}$. Drop volume $\approx 8 \mu\text{L}$. **b**, The measurement was performed at a constant velocity of $251 \mu\text{m/s}$. Drop volume $\approx 1.0 \mu\text{L}$. Notably, for liquid-like PDMS the threshold force equals the kinetic force, $F_{Th} = F_{KIN}$.

The reason for a static-kinetic transition is caused by contact angle hysteresis. This hysteresis is present for real surfaces and absent in simulations. The relatively slow transition (relaxation) from static to kinetic regime is caused by the deformability of droplets. Moving the substrate causes pronounced elongation of the droplets (see Fig. 2, Fig. S5 - Fig. S10). Such a deformation is absent in solid-solid friction.

Distinct pinning points

Large scale heterogenic surfaces resulting in distinct pinning points will lead to position dependent advancing and receding contact angles. Then the lateral adhesion forces do not develop steadily as a function of time (Figure S12). In the particular case presented in Figure S12 the lateral forces in the kinetic regime can be even higher than the one at the threshold, i.e. these surfaces do not show a well-defined threshold and a well-defined kinetic regime as the drop undergoes pronounced stick-slip motion. The drop gets stuck for several seconds until another threshold force is overcome. Large scale heterogenic or dirty surfaces (Figure S12) are associated with an irregular appearance of maxima and minima in the kinetic regime. Thus, the presented measurement provides quantitative information on the cleanliness of a surface.

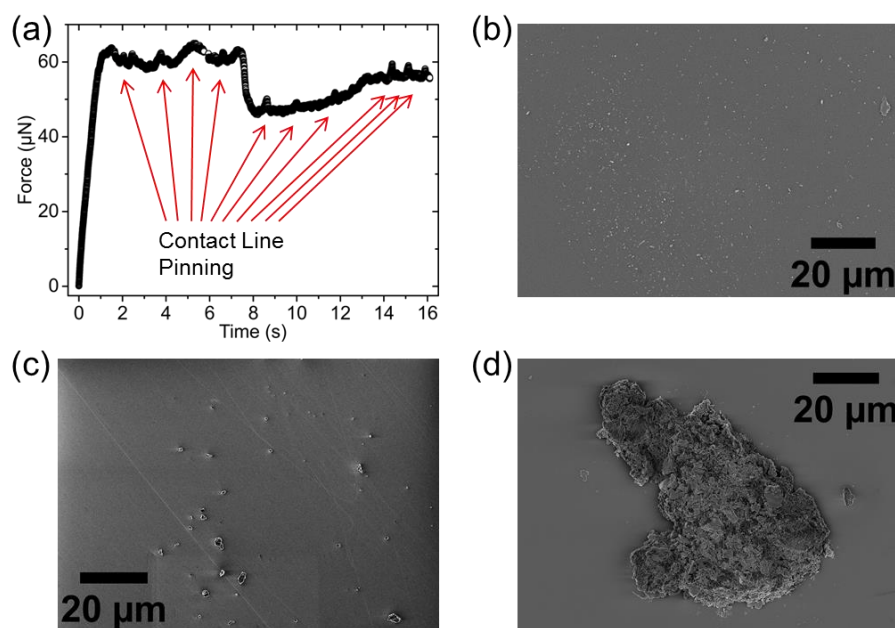


Figure S12. Distinct pinning points. (a) Force development of a water drop on a Si wafer substrate that had surface inhomogeneities due to insufficient cleaning. The red arrows indicate the force fluctuations in the kinetic regime caused by contact line pinning. The size of the drop is around 7.5 μL . The velocity of the drop is 0.94 mm/s. Scanning Electron Microscopic images reveal that scattered particles (b), coating streaks (c) and particle clusters (d) constitute the surface defects on a Si wafer substrate, which could cause significant contact line pinning and therefore force fluctuations.

Dependence on contact width

The kinetic and the threshold forces show a linear dependence on the contact width, L , of drops (Figure S13). The lateral adhesion force of different drop sizes can be directly compared by calculating the ratio of F_{LA} and L :

$$F_{LA}/L = k \cdot \gamma \cdot (\cos \theta_{\text{Rear}} - \cos \theta_{\text{Front}})$$

The linear dependence is also valid at different velocities for both the threshold force and the kinetic force (Figure S13).

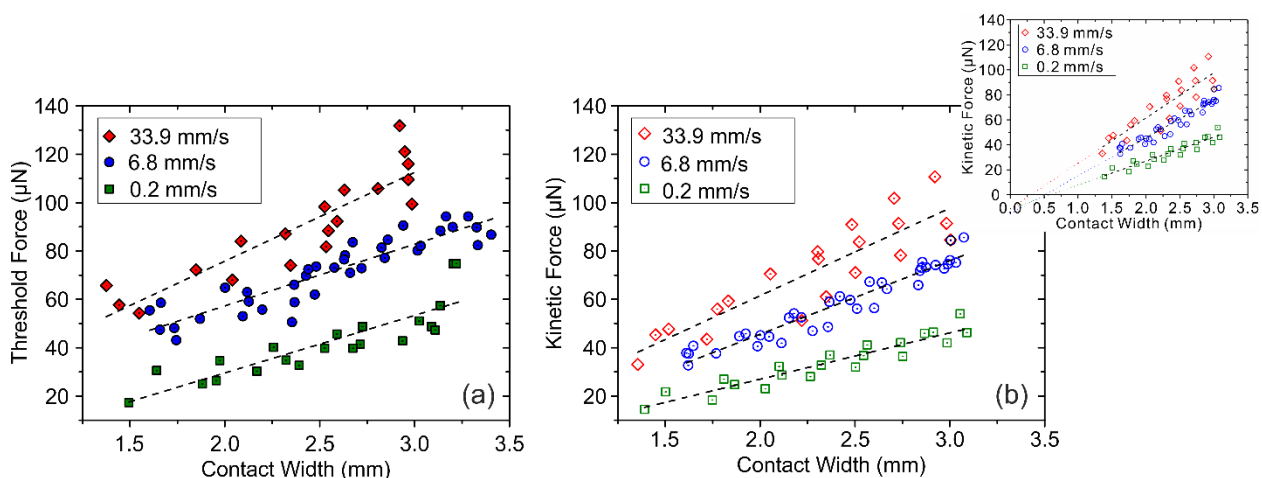


Figure S13 Dependence on contact width. Lateral adhesion forces at the threshold (a) and in the kinetic regime (b), respectively, as a function of contact width for water drops moving on a fluorinated Si wafer substrate at three velocities: 0.2 mm/s, 6.8 mm/s and 33.9 mm/s. The dotted lines are linear fits to the data. Inset: The linear fits to the data were extrapolated to a contact width of 0. The slopes are $36 \pm 4 \mu\text{N}/\text{mm}$ for 33.9 mm/s, $30 \pm 2 \mu\text{N}/\text{mm}$ for 6.8 mm/s, and $19 \pm 2 \mu\text{N}/\text{mm}$ for 0.2 mm/s. The y-intercepts are approximately $-11 \pm 10 \mu\text{N}$ for 33.9 mm/s, $-15 \pm 4 \mu\text{N}$ for 6.8 mm/s, and $-11 \pm 4 \mu\text{N}$ for 0.2 mm/s.

(2-11) Dependence on velocity

To investigate the dependence of the lateral adhesion force on velocity, we used a combination of three different motion stages. This enables us to vary the velocity by almost five orders of magnitude, i.e. from 2 $\mu\text{m/s}$ to 33 mm/s . For high velocities the adhesion forces in the kinetic regime (F_{KIN}) and at the threshold (F_{THRD}) increase with the velocity. For low velocities the lateral adhesion force remained constant.

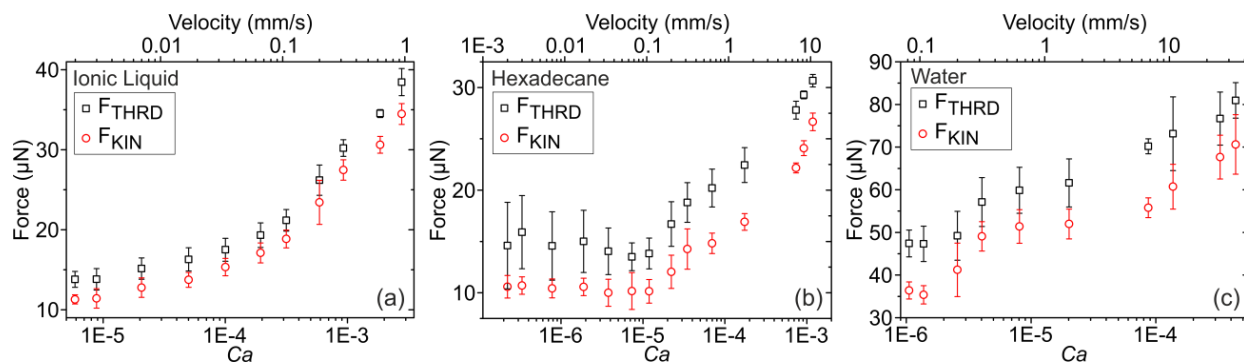


Figure S14. Velocity dependence of the lateral adhesion force. (a) Ionic liquid (1-butyl-2,3-dimethylimidazolium bis(trifluoromethanesulfonyl)imide) drop ($\approx 2 \mu\text{L}$) on a fluorinated Si wafer substrate. (b) Hexadecane drops ($\approx 3 \mu\text{L}$) on a fluorinated Si wafer substrate. (c) Water drops ($\approx 7.5 \mu\text{L}$) on a fluorinated Si wafer substrate. For water, velocities below 0.08 mm/s were not studied owing to evaporation of water and therewith related changes in drop size. The fluorination of Si wafer substrates was performed in solutions mixed with PFDTs (1H,1H,2H,2H-perfluorodecyltrichlorosilane) and n-hexane. The error bars correspond to the standard deviation calculated from 5 - 7 independent measurements.

Note, the absolute values for the lateral adhesion forces sensitively depend on the surface chemistry, thus they can be used to quantify the quality of a substrate. The highest velocity that can be probed is given by the threshold force where the liquid drop detaches from the glass capillary ($\approx 81 \mu\text{N}$ for water, $\approx 36 \mu\text{N}$ for ionic liquid and $\approx 31 \mu\text{N}$ for hexadecane).

Green-Kubo relation for friction at liquid-solid interfaces

Huang & Szlufarska “developed a Green-Kubo relation that enables accurate calculations of the coefficient of friction $\bar{\eta}$ at solid-liquid interfaces directly from equilibrium MD simulations and that provides a pathway to bypass the time-scale limitations typical for nonequilibrium MD simulations.”¹ However, these calculations do not consider contributions to friction at the three-phase contact line of drops.

In order to compare our measurements to this Green-Kubo relation, we estimated the slip length, the slip velocity and finally the friction force based on the equations provided in the manuscript by Huang & Szlufarska.

Huang & Szlufarska defined a friction coefficient $\bar{\eta} = \eta/l$, where η is the viscosity of the liquid and l is the slip length. The time step for the simulation was set to be 0.002τ , where $\tau = \sqrt{\frac{m\sigma^2}{\epsilon}}$.

Here, m is the mass of the liquid particle, σ is a characteristic length, and ϵ is the energy in Lennard Jones units. The bond strength between the solid wall and the liquid particle is $\epsilon_b = a\epsilon$, where a varied between 0.1 and 0.6. Huang & Szlufarska reported a linear dependence of the friction coefficient with the bond strength, i.e. $\bar{\eta} = k \frac{\epsilon \tau}{\sigma^4}$ (Figure 4 in the paper of K. Huang and I. Szlufarska). For hard sphere particles the values for k varied between 0.3 and 1. Inserting τ yields:

$$\bar{\eta} = k \frac{\epsilon \tau}{\sigma^4} = k \frac{\sqrt{\epsilon m}}{\sigma^3}. \text{ This results in a slip length of: } l = \frac{\eta}{\bar{\eta}} = \frac{\eta}{k} \frac{\sigma^3}{\sqrt{\epsilon m}}.$$

In order to quantify the slip length, we converted the quantities given in Lennard Jones units to experimental values. It should be noted, that here some uncertainties exist. Therefore we consider only the order of magnitudes.

For a drop of water ($m \approx 3 \times 10^{-26}$ kg) on a hydrophobic surface we estimated the characteristic length as $\sigma \approx \left(\frac{m}{\rho}\right)^{\frac{1}{3}} = \left(\frac{3 \cdot 10^{-26} \text{ kg}}{1000 \text{ kg m}^{-3}}\right)^{\frac{1}{3}} \approx 3 \cdot 10^{-10} \text{ m}$ and the energy as $\epsilon = 1k_B T$. This results in a variation of the bond strength between $(0.1 \dots 0.6)k_B T = (0.4 \dots 2.4) \cdot 10^{-21} \text{ Nm}$. The bulk viscosity of water is: $\eta = 10^{-3} \text{ Pa s}$. Depending on the bond strength, the slip length for water is then:

$$l = \frac{\eta}{k} \frac{\sigma^3}{\sqrt{\epsilon m}} = \frac{10^{-3} \text{ Pa s}}{(0.3 \dots 1)} \frac{(3 \cdot 10^{-10} \text{ m})^3}{\sqrt{4 \cdot 10^{-21} \text{ Nm} \cdot 3 \cdot 10^{-26} \text{ kg}}} \approx 2 \dots 8 \text{ nm}.$$

This agrees with our previously published measurements, showing that the slip length should be $< 10 \text{ nm}^2$.

The next step is to quantify the forces associated with the slip length. The slip velocity used for the MD simulations is given as: $u \approx \frac{\sigma}{\tau} = \sqrt{\epsilon/m}$. Huang & Szlufarska varied the slip velocity from 0.01 to $0.6\sigma/\tau$ or 0.01 to $0.6\sqrt{\epsilon/m}$, respectively. Thus, the slip velocity was varied between $u \approx (4 \dots 200) \text{ m/s}$. For drops with heights in the order of mm and a 10 nm slip length, a drop velocity relative to the substrate of $v_{drop} = \frac{h_{drop} + l}{l} \cdot u \approx 4 \cdot 10^5 \text{ m/s} \dots 2 \cdot 10^7 \text{ m/s}$ is obtained. On one hand, this value is more than seven magnitudes higher than our experimental realized substrate velocities ($3 \cdot 10^{-2} \text{ m/s}$). On the other hand, for our experimental velocity range, we can use the equation to back calculate a slip velocity of $3 \cdot 10^{-7} \text{ m/s}$.

The friction force per unit area is defined by $F = -\bar{\eta}u$, which is now used to calculate the force per unit area for a slip length l of 10 nm:

$$|F| = \bar{\eta}u = \frac{\eta u}{l} \approx \frac{10^{-3} \text{ Pa s}}{10 \text{ nm}} \cdot 3 \cdot 10^{-7} \text{ m/s} = 0.03 \frac{\text{N}}{\text{m}^2}$$

This yields for the friction force $|F| * A \approx 0.03 \frac{\text{N}}{\text{m}^2} \cdot 3 \cdot 10^{-6} \text{ m}^2 \approx 1 \cdot 10^{-7} \text{ N}$, where A is the liquid-solid contact area of the droplet (radius of 1 mm).

For a sliding water drops on planar surfaces we measured forces $> 10 \mu\text{N}$ (water on fluorinated Si wafer substrate, Figure 4). Thus the contribution of viscous friction force due to slips is small. The major contribution to the force measured arises from contact line friction.

Rolling versus sliding

In order to find out if the liquid drop movements correspond more to rolling or sliding we have performed experiments where we have used a water-D₂O 1:1 mixture with polystyrene (PS)

particles having diameters from 50 to 200 μm . The PS particles acted as tracers to follow the motion of the liquid. Figure S15 shows snapshots for a drop moving a fluorinated Si wafer (a) and a PDMS brush grafted liquid like surface (LLS) (b) studied at two different velocities of 0.125 mm/s ($\text{Ca} = 1.8 \cdot 10^{-6}$) and 4 mm/s ($\text{Ca} = 6 \cdot 10^{-5}$).

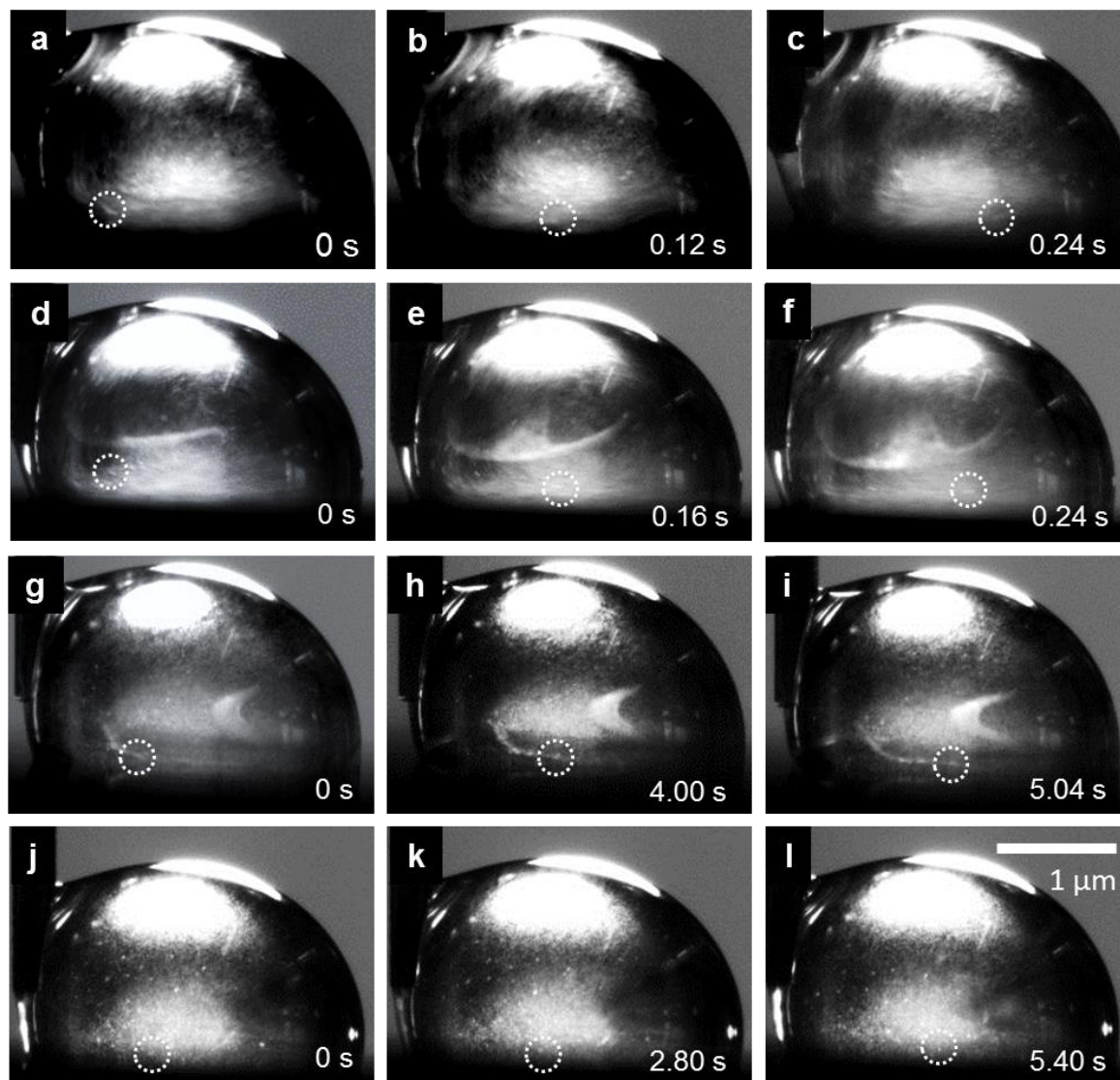


Figure S15: Drops (7.5 μl) of water- D_2O mixture (1:1) moving on a fluorinated Si surface with velocities of (a-c) 4 mm/s and (g-i) 0.125 mm/s, and on a PDMS brush grafted surface (liquid like surface) with velocities of (d-f) 4mm/s and (j-l) 0.125 mm/s.

Based on this series of experiments we calculated the relative velocities of the particles close to the substrate interface

sample	stage speed	Particle speed
Fluorinated Si wafer	4 mm/s	3.9 ± 0.9 mm/s
	0.125 mm/s	0.13 ± 0.05 mm/s
Liquid-Like surface	4 mm/s	3.0 ± 0.8 mm/s
	0.125 mm/s	0.08 ± 0.05 mm/s

These measurements indicate that the motion of liquid drops is dominated by rolling (Supplementary Movies 8-11). This is in agreement with Fig. S13. The linear extrapolations of the kinetic force dependence suggest a linear dependence with an intercept slightly below zero force. Therefore we conclude that the liquid drop friction is dominated by contact line friction and interfacial friction only plays a minor role.

Velocity dependence of the goose feather

For the water-feather interface, the lateral adhesion forces at the threshold and in the kinetic regime did not change significantly with velocity. For drops on structured, hydrophobic surfaces, in particular superhydrophobic surfaces, viscous dissipation is low. Energy is mainly dissipated by depinning from surface protrusions. In the measured velocity range, the drop showed pronounced pinning and depinning events, causing large variations of the threshold and kinetic force. Notably, the lateral adhesion force does not depend on velocity within experimental accuracy (Figure S16). The surface texture and the flexibility of the goose feather might cause this peculiar behaviour. The feather’s flexibility allows adapting its shape to the liquid drop.

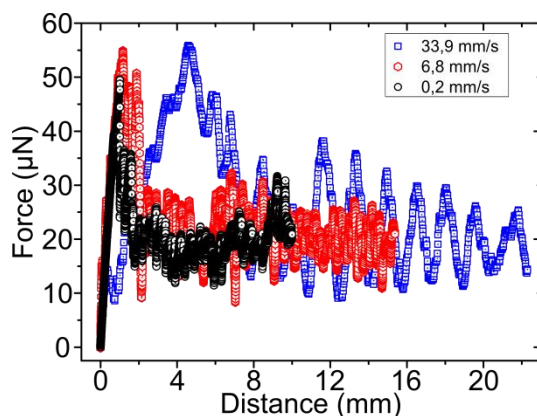


Figure S16. Lateral adhesion force of a goose feather. Representative of the lateral adhesion forces as a function of distance the substrate travels under three velocities, 0.2 mm/s, 6.8 mm/s, and 33.9 mm/s. The scattering of the data points is caused by a variation of topographic features of the surfaces.

Error estimation of our data

Error for the lateral adhesion force: The error for the lateral adhesion force measurement corresponds to 5% and arises from calibrating the spring constant of the borosilicate capillary and the sensitivity of the PSD (Fig. 5 in Dynamic Measurement of the Force Required to Move a Liquid Drop on a Solid Surface, Langmuir, Pilat *et al.*, 2012)³. The error in the spring constant measurement is <1%. After repeating the calibration for three times, an average spring constant of 0.202 ± 0.002 N/m is obtained. The standard deviation is <1% of the average. This error corresponds to the size of the symbols used in the plots of Figures 2a, 3a, and 5b.

The maximum value of the lateral adhesion coincided with the force at the threshold to movement of the drop. In the kinetic regime we calculated the mean value of the adhesion force – within the last 5 seconds at times > 20 s. The error corresponds to its standard deviation.

The error of the calculated adhesion forces corresponds to the propagation of the errors arising from the measurement of the contact widths (e.g. Fig. 2b) and the reading of the contact angles (e.g. Fig. 2c). Here the reading error of the contact angle dominates.

Error for the contact width and length: The contact widths and contact lengths were calculated from the video images. Hereby we used the capillary diameters as a scale (0.460 ± 0.046 mm for contact width and 0.10 ± 0.01 mm for contact length). The pixel size corresponds to $10 \mu\text{m}$ for the high-speed camera and $6.7 \mu\text{m}$ for the other camera. The reading error of one edge of a drop could be up to 3 pixels.

Error for the contact angles: The contact angles were also estimated from the video images. The measurement error of the contact angles was typically within 3° . The error for the front contact angle was larger for the superhydrophobic surfaces. Each data point shows an average of 3 - 4

measurements of the contact angle. The error bars are plotted in Fig. 2c and reflect the individual error in reading of each frame of the video.

(2-16) Movies (avi) of force measurements of different liquid substrate combinations

Movie 1: An ionic liquid drop moving on a fluorinated Si wafer at a velocity of 0.202 mm/s. Duration of the video is 2.58 s in real time.

Movie 2: A water drop moving on fluorinated silicone nanofilaments coated on a glass slide at a velocity of 0.202 mm/s. Duration of the video is 3 s in real time.

Movie 3: A hexadecane drop moving on a fluorinated Si wafer at a velocity of 0.202 mm/s. Duration of the video is 2.5 s in real time.

Movie 4: A water drop moving on fluorinated SU-8 pillars coated on a glass slide at a velocity of 0.202 mm/s. Duration of the video is 2.4 s in real time.

Movie 5: A water drop moving on a fluorinated Si wafer at a velocity of 0.202 mm/s. Duration of the video is 1.96 s in real time.

Movie 6: A water drop moving on fluorinated TiO₂ nanoparticles coated on a silicon wafer at a velocity of 0.202 mm/s. Duration of the video is 2.19 s in real time.

Movie 7: A water drop moving on PDMS coated on a glass slide at a velocity of 0.202 mm/s. Duration of the video is 2.5 s in real time.

Movie 8: A drop of Water-D₂O / 1:1 mixture (7.5 μl) containing polystyrene particles (diameters from 50 to 200 μm) moving on a fluorinated Si surface at a velocity of 4 mm/s. The drop is held by a needle while the substrate is moving. The polystyrene particles act as tracers to follow the motion of the liquid. The movie is accelerated by 1.65 times.

Movie 9: A drop of Water-D₂O / 1:1 mixture (7.5 μl) containing polystyrene particles (diameters from 50 to 200 μm) moving on a fluorinated Si surface at a velocity of 0.125 mm/s. The polystyrene particles act as tracers to follow the motion of the liquid. The movie is accelerated by 1.65 times.

Movie 10: A drop of Water-D₂O / 1:1 mixture (7.5 μ l) containing polystyrene particles (diameters from 50 to 200 μ m) moving on a PDMS brush grafted surface at a velocity of 4 mm/s. The movie is accelerated by 1.65 times.

Movie 11: A drop of Water-D₂O / 1:1 mixture (7.5 μ l) containing polystyrene particles (diameters from 50 to 200 μ m) moving on a PDMS brush grafted surface at a velocity of 0.125 mm/s. The movie is accelerated by 1.65 times.

References:

- 1 Huang, K. & Szlufarska, I. Green-Kubo relation for friction at liquid-solid interfaces. *Phys. Rev. E* **89**, 032119, (2014).
- 2 Schaeffel, D. *et al.* Hydrodynamic boundary condition of water on hydrophobic surfaces. *Phys. Rev. E* **87**, 051001, (2013).
- 3 Pilat, D. W. *et al.* Dynamic Measurement of the Force Required to Move a Liquid Drop on a Solid Surface. *Langmuir* **28**, 16812-16820, (2012).